Supplement of Nat. Hazards Earth Syst. Sci., 25, 1229–1253, 2025
https://doi.org/10.5194/nhess-25-1229-2025-supplement

Natural Hazards and Earth System Sciences
Open Access
EGU

Supplement of

Topographic controls on landslide mobility: modeling hurricane-induced landslide runout and debris-flow inundation in Puerto Rico

Dianne L. Brien et al.

Correspondence to: Dianne L. Brien (dbrien@usgs.gov)

This supplement includes specific technical information describing channel network delineation, application of a bandpass filter to derive flow directions, description and flowchart describing connections between the topographic analysis and linked-model approach, and statistics from the topographic analysis of mobility zones.

S1 Channel network delineation

Delineation of a channel network derived from the 1 m DEMs was essential for derivation of flow direction and flow accumulation for runout modeling, as well as the distinction of non-channelized versus channelized runout zones. Roads are an inherent problem for channel detection algorithms that use high-resolution topographic data, as roads often obscure the topography of natural channels. In Puerto Rico, large municipal roads, along with small agricultural and private roads (Ramos-Scharrón et al., 2021), led to significant disruption of the flow directions derived from the DEMs. Whereas some debris flows from Hurricane Maria were diverted by these agricultural roads, the majority bypassed roads and continued down natural channels (Bessette-Kirton et al., 2019a). Accurately modeling debris-flow inundation required defining downstream channel networks that were continuous across laterally intersecting road networks.

Our automated methods applied two strategies to eliminate road-network artifacts from the lidar-derived DEMs and construct channel networks representative of natural channels from the lidar-derived DEM: 1) identification of the location of channel initiation using a curvature-based flow accumulation threshold, and 2) spectral filtering of the DEMs to remove road artifacts downstream of channel initiation.

S1.1 Curvature-based method to identify channel initiation

Our implementation of curvature-based network delineation was inspired by Tarboton and Ames (2001) and used a flow accumulation threshold including only topographic concavities (hollows) that are representative locations of channel initiation. To detect channel initiation points for our drainage network, we used concave planform curvature to identify areas representative of topographic hollows.

Steps in our method to identify locations of channel initiation included: 1) using a local mean to smooth the DEM, 2) calculating planform curvature, 3) applying a curvature threshold to identify concavities in the topography, 4) eliminating small, isolated concavities, 5) calculating the contributing area of remaining concavities, and 6) applying an area threshold using only the contributing area of concave topography. We used threshold values based on topographic scaling factors and published values (Pelletier, 2013; Mudd et al., 2019). The location of channel initiation was assigned where the contributing concave area, defined as a planform curvature > 0.02 m^{-1}, was larger than 500 m^2. This method of channel network delineation is available in Grfin Tools (Cronkite-Ratcliff et al., 2025; Reid et al., 2025).

S1.2 Bandpass DEM to derive flow directions

In areas downstream of channel initiation, the channel network and associated flow directions from the lidar-derived DEMs were sometimes diverted at road intersections. We employed a spectral filtering approach to remove small roads from the topography. Using SpecFiltTools software (Perron et al., 2008), we applied a Gaussian bandpass filter to remove topographic features at the wavelength of small agricultural roads (~10 m) while retaining both the smaller and larger wavelengths that constitute the undisturbed topography. The combination of our two strategies provided an automated method to remove small roads from channel networks over diverse geomorphic and geologic terranes.

S2 Topographic analysis

S2.1 Connections between topographic analysis and linked-model approach

The topographic analysis guided selection of input parameters for the linked-model and our decision to apply the same parameters for all geologic terranes. Figure S1 shows a flowchart illustrating details of the steps performed for channel network derivation (described in S1) and the topographic analysis (S2) as they relate to components of the linked model: non-channelized runout (yellow) and debris-flow inundation (purple). Blue boxes indicate existing data sources.

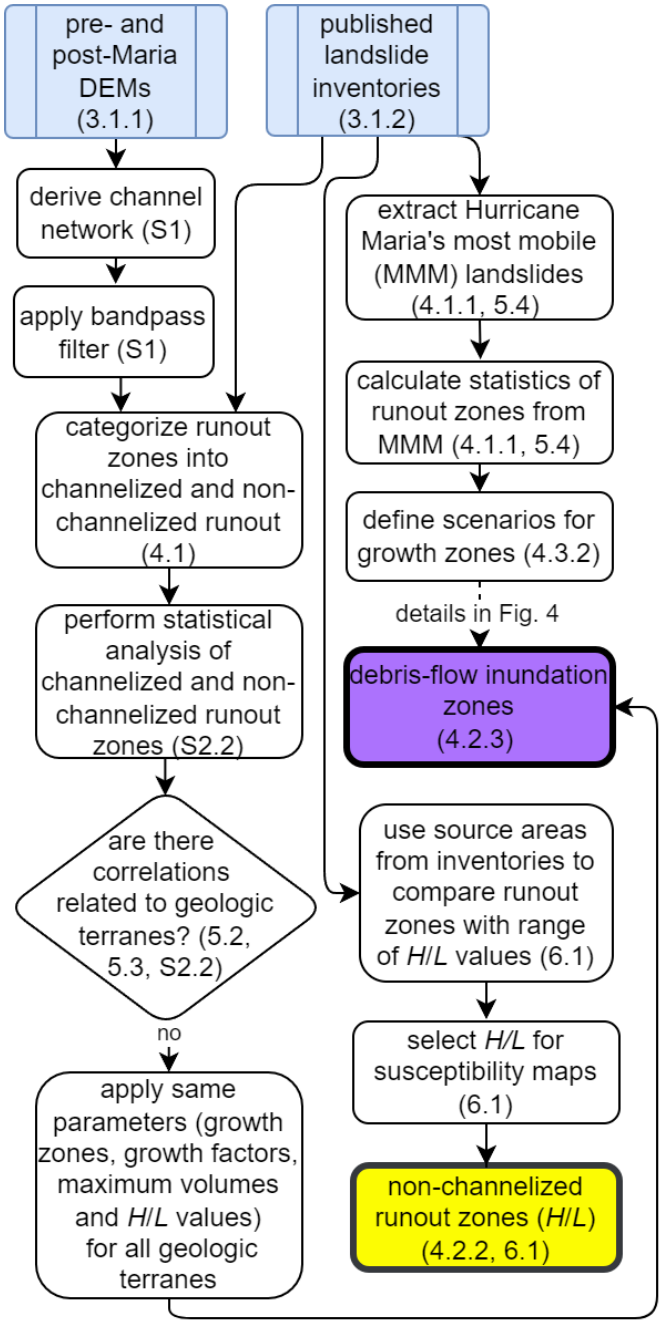

Figure S1. Flowchart of our topographic analysis and connections to two components of the linked model. Blue boxes indicate published data sources. Yellow and purple boxes indicate components of our linked-model approach

S2.2 Topographic analysis of mobility zones

Within the three mobility zones, we: 1) evaluated the percentage of each study area encompassed by each zone, 2) analyzed summary statistics to compare the distribution of topographic slopes in the three mobility zones, and 3) compared variability between study areas. Summary statistics were analyzed based on every raster cell within a mobility zone.

To evaluate the percentage of each study area affected by landslide source zones, we considered: 1) percentage of full study area, and 2) percentage of each study area susceptible to landslides, approximated by steep slopes greater than 30° (Coe et al., 2021). This approximation of susceptible areas was consistent with field observations of Baum et al. (2018), and provides a rational criterion to calculate normalized values, whereby, the percentage of area affected would be similar across all study areas if all other contributing factors were equal.

Summary statistics, for each mobility zone in each study area, included percentiles and the adjusted Fisher-Pearson coefficient of skewness (G_1) (Zwillinger and Kokoska, 2000), a measure of the asymmetry of a statistical distribution, where $-0.5 < G_1 < 0.5$ indicates the data are approximately symmetric; $-1 < G_1 < -0.5$ indicates the data are moderately left-skewed; $0.5 < G_1 < 1$ indicates the data are moderately right-skewed; $G_1 < -1$ indicates the data are highly left-skewed; $G_1 > 1$ indicates the data are highly right-skewed (Brown, 2022).

Table S1. Percentile statistics of extreme (P_{10}) and average (P_{50}) slopes, in degrees, and the adjusted Fisher-Pearson coefficient of skewness (G_1) (Zwillinger and Kokoska, 2000) for slopes in the entire study areas and mapped landslide-affected areas, divided into the three zones of landslide mobility. The nine study areas are ordered by increasing percentage of area susceptible to landslides. This order also corresponds with the same order as the median slope of the entire study area (column 2).

symbol	study area name	entire study area			source zone			non-channelized runout			channelized runout		
		P_{10} (1)	P_{50} (2)	G_1 (3)	P_{10} (4)	P_{50} (5)	G_1 (6)	P_{10} (7)	P_{50} (8)	G_1 (9)	P_{10} (10)	P_{50} (11)	G_1 (12)
⬢	U5	4.1	20.7	-0.89	23.1	38.6	0.16	13.4	29.6	-0.59	10.4	23.3	-0.54
■	U3	7.5	24.1	-0.77	29.3	40.4	1.55	16.5	34.5	-0.18	12.2	27.5	-0.73
■	U4	7.7	24.7	-0.61	30.2	40.8	2.12	14.9	31.4	-0.24	11.0	27.5	-0.72
▲	L3	12.1	26.7	-0.41	25.5	36.7	0.72	16.0	29.9	-0.37	13.6	27.8	-0.51
●	N	9.7	27.8	-0.46	25.5	35.6	0.86	12.6	29.6	-0.14	10.1	26.2	-0.71
▲	L1	10.1	28.6	-0.70	29.0	40.0	1.75	21.9	37.5	0.52	17.0	34.1	-0.46
◆	U2	12.5	30.9	-0.18	28.3	37.8	1.39	17.5	32.4	0.62	13.5	29.7	-0.45
▲	L2	11.8	31.4	-0.43	31.6	41.1	2.56	23.8	39.0	1.08	17.9	34.7	-0.47
◆	U1	9.5	32.8	-0.35	30.5	40.2	1.69	19.0	35.8	1.13	11.0	27.0	-0.69

Table S2. Minimum, maximum, mean, and standard deviation of P_{10} and P_{50} in the nine study areas (Table 4) for slopes (in degrees) in the entire study areas and for mapped landslide-affected areas, divided into the three zones of mobility.

	entire study area		source zones		non-channelized runout		channelized runout	
	P_{10} (1)	P_{50} (2)	P_{10} (3)	P_{50} (4)	P_{10} (5)	P_{50} (6)	P_{10} (7)	P_{50} (8)
minimum	4.1	20.7	23.1	35.6	12.6	29.6	10.1	23.3
maximum	12.5	32.8	31.6	41.1	23.8	39.0	17.9	34.7
mean	9.7	27.8	29.0	40.0	16.5	32.4	12.2	27.5
standard deviation (σ)	2.7	3.9	2.8	1.9	3.7	3.6	2.8	3.7

Variability between median (P_{50}) source-zone slopes in nine study areas was minimal, ranging from 35.6 to 41.1°, with a standard deviation (σ) of 1.9° (Table S2, column 4). In contrast, median slopes within the study areas, non-channelized and channelized runout zones (Table S1) showed almost twice the variability (σ = 3.9, 3.6, and 3.7°, respectively) (Table S2, columns 2, 6, 8). Extreme (P_{10}) values for study areas, source zones, non-channelized runout, and channelized runout (Table S1) displayed slightly higher variability (σ = 2.7, 2.8, 3.7, and 2.8°, respectively) between study areas (Table S2, columns 1, 3, 5, 7), compared to P_{50} of source-zones.

For overall study area slopes, skewness ranged from approximately symmetric (L3, N, U2, L2, U1) to moderately left skewed (U3, U4, U5, L1) (Table S1, column 3). The upland terrains (U3, U4) had left-skewed distributions of slopes. Slopes of source zones varied from approximately symmetric (U5) to moderately (L3, N) to highly right skewed (U1, U2, U3, U4, L1, L2) (Table S1, column 6). The distribution of slopes in areas of non-channelized runout was moderately left skewed to highly right skewed (Table S1, column 9) and channelized runout was approximately symmetric (L1, U2, L2) to moderately left skewed (U1, N, L3, U3, U4, U5) (Table S1, column 12). Our results indicate there was no clear pattern in slope characteristics of landslide-affected areas related to geologic terrane or geomorphic terrain.

Results also show median source-zone slopes were not correlated with median slopes of the study area (Fig. S2a); instead, they were relatively consistent across all study areas. There was some correlation between slopes of non-channelized runout zones (P_{10} and P_{50}) and median slope of study area (Fig. S2b).

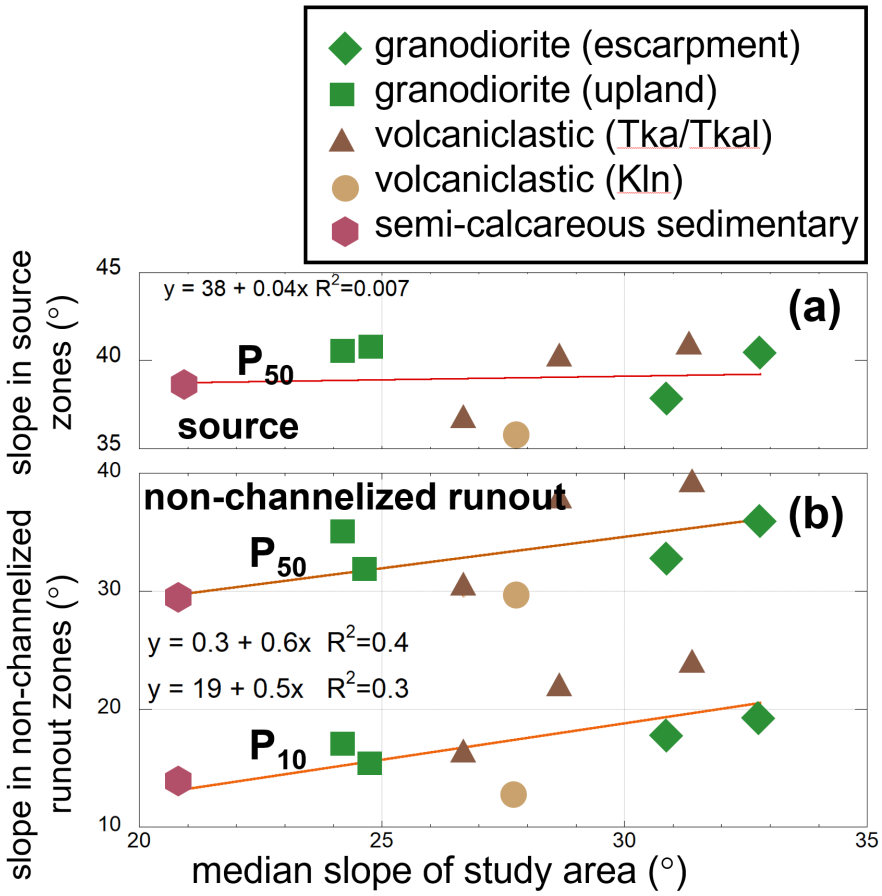

Figure S2. Median slope of study area related to slopes of a) landslide source zones and b) non-channelized runout zones.

References

Baum, R.L., Cerovski-Darriau, C., Schulz, W.H., Bessette-Kirton, E.K., Coe, J.A., Smith, J.B., and Smoczyk, G.M.: Variability of Hurricane Maria debris-flow source areas in Puerto Rico—Implications for hazard assessment, American Geophysical Union Fall Meeting abstract #NH14A-02, 2018.

Bessette-Kirton, E.K., Cerovski-Darriau, C., Schulz, W.H., Coe, J.A., Kean, J.W., Godt, J.W., Thomas, M.A., and Hughes, K.S.: Landslides triggered by Hurricane Maria: Assessment of an extreme event in Puerto Rico, GSA Today, 29(6), 4-10, https://doi.org/10.1130/GSATG383A.1, 2019a.

Brown, S.: Measures of Shape: Skewness and Kurtosis, https://Brownmath.com/Stat/Shape.htm , last access: 23 March 2022

Coe, J.A., Bessette-Kirton, E.K., Brien, D.L., and Reid, M.E.: Debris-flow growth in Puerto Rico during Hurricane Maria: Preliminary results from analyses of pre- and post-event lidar data, in Cabrera MA, Prada-Sarmiento LF, Montero J, (Eds.), Proceedings of the 13th International Symposium on Landslides, Cartagena, Colombia, International Society for Soil Mechanics and Geotechnical Engineering, 8 p., https://www.issmge.org/uploads/publications/105/106/ISL2020-7.pdf., last access: 9 March 2022, 2021.

Cronkite-Ratcliff, C., Reid, M.E., Brien, D.L., and Perkins, J.P.: Grfin — Software package and runtime documentation for users, version 1.0, U.S. Geological Survey Software Release, https://doi.org/10.5066/P9NVKFE2,2025.

Mudd, S.M., Clubb, F.J., Grieve, S.W.D., Milodowski, D.T., Hurst, M.D., Gailleton, B., and Valters, D.A.: Lsdtopotools2, Zenodo, https://doi.org/10.5281/zenodo.3245041, 2019.

Pelletier, J.D.: A robust, two-parameter method for the extraction of drainage networks from high-resolution digital elevation models (DEMs): Evaluation using synthetic and real-world DEMs, Water Resources Research, 49(1), 75-89. https://doi.org/10.1029/2012WR012452, 2013.

Perron, J.T., Kirchner, J.W., and Dietrich, W.E.: Spectral signatures of characteristic spatial scales and nonfractal structure in landscapes, Journal of Geophysical Research, Earth Surface, 113(F4), https://doi.org/10.1029/2007JF0008662, 2008.

Ramos-Scharrón, C.E., Arima, E.Y., Guidry, A., Ruffe, D., and Vest, B.: Sediment mobilization by hurricane-driven shallow landsliding in a wet subtropical watershed, Journal of Geophysical Research, Earth Surface, 126(5), https://doi.org/10.1029/2020JF006054, 2021.

Reid, M.E., Brien, D.L., Cronkite-Ratcliff, C., and Perkins, J.P.: Grfin Tools — User guide and methods for modeling landslide runout and debris-flow growth, and inundation, U.S. Geological Survey Techniques and Methods, book 14, chap. A3, https://doi.org/10.3133/tm14-A3, 2025.

Tarboton, D.G., and Ames, D.P.: Advances in the mapping of flow networks from digital elevation data, In Bridging the Gap: Meeting the World's Water and Environmental Resources Challenges, 1-10, https://doi.org/10.1061/40569(2001)166, 2001.

Zwillinger, D., and Kokoska, S.: CRC Standard Probability and Statistics Tables and Formulae, Chapman and Hall, New York, 2000, Section 2.2.24.1, 2000.